A coupled-cluster study of photodetachment cross sections of closed-shell anions

Janusz Cukras, Piero Decleva, and Sonia Coriani

Citation: The Journal of Chemical Physics **141**, 174315 (2014); doi: 10.1063/1.4900545
View online: https://doi.org/10.1063/1.4900545
View Table of Contents: http://aip.scitation.org/toc/jcp/141/17
Published by the American Institute of Physics

A coupled-cluster study of photodetachment cross sections of closed-shell anions

Janusz Cukras, Piero Decleva, and Sonia Coriani[a)]
Dipartimento di Scienze Chimiche e Farmaceutiche, Università degli Studi di Trieste, via L. Giorgieri 1, I-34127, Trieste, Italy

(Received 10 June 2014; accepted 16 October 2014; published online 6 November 2014)

We investigate the performance of Stieltjes Imaging applied to Lanczos pseudo-spectra generated at the coupled cluster singles and doubles, coupled cluster singles and approximate iterative doubles and coupled cluster singles levels of theory in modeling the photodetachment cross sections of the closed shell anions H^-, Li^-, Na^-, F^-, Cl^-, and OH^-. The accurate description of double excitations is found to play a much more important role than in the case of photoionization of neutral species.
 [http://dx.doi.org/10.1063/1.4900545]

I. INTRODUCTION

The term photoionization collectively indicates processes in which one photon is absorbed and one electron is ejected (or removed into the continuum) from the system undergoing the process. Genuine ionization conventionally corresponds to the process where a neutral system is transformed into a positive (molecular or atomic) ion, whereas if the electron is ejected ("ionized") from a negative anion the process is usually referred to as "photodetachment."

Molecular photoionization processes are basic probes of structural and dynamical properties of many-body systems, and are of interest in a variety of contexts, e.g., astrophysics, aeronomy, radiation chemistry, environmental and atmospheric chemistry, metrology, surface science, catalysis, and new material development.[1–5] Photoionization cross sections are used, for instance, in the determination of the ionization structure of cosmic gas subjected to ultraviolet and X-ray radiation.[1,2] Accurate absolute photoabsorption and total photoionization cross sections over wide spectral regions are also required for use in modeling studies. Total and partial photoionization cross sections are therefore attracting continuous attention, both experimentally and theoretically. In the specific case of photodetachment, to produce sizable amounts of stable anions on which to perform the measurements can prove very challenging, and theoretical results are therefore even more desirable. On the other hand, negative atomic ions play an important role in various branches of physics, from astrophysics, atmospheric, and plasma physics to surface physics, and accelerator physics. They are also used for dating samples of archaeological or geophysical interest, oceanography, hydrology, and biomedicine.[6]

Correlation effects are of special importance in anion photodetachment.[7–9] The process is more closely related to electron scattering processes since in both cases a neutral target is seen by the scattered electron with the same continuum structure. Notably, the absence of the static Coulomb contribution to the long range potential makes the weaker polarization and dispersion forces prominent in this case. The hydride anion H^- itself, the smallest system in which electron correlation exists, has often served as a testing system for correlated methods. As noted for instance by Balling *et al.*,[7] correlation ensures the actual binding of the ground state, so the description of the process of photodetachment is particularly sensitive to the correct description of the correlation energy. This has also been found true for the Lithium anion,[10] as well as for other systems.[8] The cross-section profiles over the ionization threshold usually reveal some structure owing to two-electron processes in which one electron is removed from the anion and the other is excited. All this puts stringent requirements on the correlation methods employed in calculations.

We have recently presented a computational study of the total photoionization cross sections of a few atoms and molecules for the hierarchy of Coupled-Cluster approximations CCS (coupled cluster singles), CC2 (coupled cluster singles and approximate doubles), and CCSD (coupled cluster singles and doubles).[11] Here we extend our previous investigation to also encompass the photodetachment cross sections of a series of (closed-shell) anions, namely, the hydride anion H^-, the alcaline anions Li^- and Na^-, the halogen anions F^- and Cl^-, and the molecular hydroxide anion OH^-.

The methodology adopted here as in Ref. 11 applies Stieltjes imaging[12–14] (aka moment theory) to a discretized representation of the continuum (the so-called pseudo-spectrum) obtained from diagonalization of a truncated tridiagonal representation of the Coupled Cluster Jacobian matrix generated using an asymmetric Lanczos algorithm for computing (complex) linear response functions.

The application of the Stieltjes imaging technique to L^2 *ab initio* methods to describe bound-continuum transitions has a long history, and several examples can be found in the literature, for example, the studies of Carravetta, Ågren, and coworkers[10,15–18] on both photoionization and photodetachment processes, Auger transition rates, and molecular shake-off continua at the Multiconfigurational Self Consistent Field level of theory. We refer to the overview by Müller-Plathe and Diercksen for further references.[14]

In principle, Stieltjes imaging would require that one uses the whole pseudo-spectrum generated from diagonalization

a)Author to whom correspondence should be addressed. Electronic mail: coriani@units.it

of the full Hamiltonian matrix, clearly a severe bottleneck for large systems. Our method is, in spirit, analogous to the one proposed by Averbukh and co-workers[19–24] within the Algebraic Diagrammatic Construction (ADC) family of propagator methods, as it applies a Lanczos algorithm in order to generate a truncated representation of the Coupled Cluster Jacobian of much smaller dimension than the full Jacobian, hereby overcoming the above mentioned bottleneck.

Our purpose here is, on one side, to test the performance and accuracy of our methodology in the case of photodetachment, with reference to both the description of correlation effects, the choice of basis sets for the representation of bound and continuum states and the order in moment theory, and, on the other side, to supply reference theoretical results for further computational and experimental investigations, also in a broader energy region than the one that has been experimentally covered to date.

II. METHODOLOGY

The computational protocol employed both here and in our previous study[11] is rooted on the well-known "moment theory," developed by Chebyshev, Markov, Stieltjes, and others,[14] often referred to as Stjelties imaging. An excellent review on Stieltjes imaging is given in Ref. 14. Below we summarize the essential points.

First of all, the absorption cross section $\sigma(\omega)$ is the probability for a photon of energy ω to be absorbed. It is proportional to the (differential) oscillator strength $f(\omega)$,

$$\sigma(\omega)[\mathrm{Mb}] = 2\pi^2 \alpha a_0^2 \times 10^{18} f(\omega), \tag{1}$$

where α is the fine structure constant, a_0 is the Bohr radius in centimeters, and $1\ \mathrm{Mb} = 10^{-18}\ \mathrm{cm}^2$.

When one refers to "simple" photoabsorption from $|0\rangle$ to $|i\rangle$, one usually considers the individual (discrete) oscillator strengths f_i at (discrete) photoabsorption energy ω_i. When one deals with photoionization, however, the discrete f_i are replaced by a continuous *oscillator strength function* $f(\omega)$, which in the dipole-gauge is given by

$$f(\omega) = \frac{2}{3} \left| \langle 0|\mu|\phi(\omega)\rangle \right|^2, \tag{2}$$

where $\phi(\omega)$ is a continuum solution of the Schrödinger equation. The continuum solutions form a continuous spectrum, whereas the bound solutions form a discrete set. The continuum and discrete wavefunctions satisfy different boundary conditions.

The *moments* $s(k)$ of the oscillator strength are defined,

$$s(k) = \sum_{i}^{discr} \omega_i^k f_i + \int_{\omega_T}^{\infty} \omega^k f(\omega) d\omega \tag{3}$$

and are central quantities in moment theory. It is assumed that moments of the continuum oscillator strength, $S(k) = \int_{\omega_T}^{\infty} \omega^k f(\omega) d\omega$, can be approximated as sum of N discrete pseudo-states that fall into the continuum, $S(k) \approx \sum_i^N \bar{\omega}_i^k \bar{f}_i$.

In Stjelties imaging a "primitive" set of M excitation energies and oscillator strengths is transformed in order to obtain the correct representation of the continuum and energy normalization.

One first computes a number $(2r)$ of "spectral moments" $S(-k)$ of the primitive spectrum

$$S(-k) = \sum_{j=1}^{M} f_j \omega_j^{-k}; \qquad k = 0, \ldots, 2r-1, \tag{4}$$

where r is chosen *a priori*. As the pseudo-states of the primitive spectrum come from a calculation in square-integrable basis (L^2 basis), they have, above the ionization threshold, the wrong boundary conditions (those of the bound states instead of those of the continuum states), so they are physically meaningless and extremely method and basis-set dependent. However, as the basis set approaches completeness, their spectral moments $S(-k)$ converge towards the spectral moments of the true oscillator strength.

From the $2r$ spectral moments, discretized spectra of order $n = 2, \ldots, r$, called *principal* pseudo-spectra, are generated as generalized (Gaussian) quadrature points (abscissae) $\omega_j^{(n)}$ and weights $f_j^{(n)}$,

$$S(-k) = \sum_{j=1}^{n} f_j^{(n)} (\omega_j^{(n)})^{-k}; \qquad k = 0, \ldots, 2n-1. \tag{5}$$

In doing this, the cross-section has been "smoothed," as there are typically many more "raw" pairs of energies and strengths in the primitive spectrum, than quadrature points and weights in the principal spectrum. These resulting points are adapted to reproduce the lowest order spectral moments (which should be the ones more accurately reproduced by the primitive set). The Stjelties process also places the points where they are most needed, that is, the density of abscissae is higher where the cross section changes more rapidly.

From the Gaussian quadrature points and weights, one can define an approximate distribution function $F^{(n)} = \sum_{\omega_j < \omega} f_i^{(n)}$ of order n,

$$F^{(n)}(\omega) = 0, \quad \omega < \omega_1, \tag{6}$$

$$F^{(n)}(\omega) = \textstyle\sum_{j=1}^{i} f_j, \quad \omega_i < \omega < \omega_{i+1}, \tag{7}$$

$$F^{(n)}(\omega) = \textstyle\sum_{j=1}^{n} f_j = S(0), \quad \omega_n < \omega. \tag{8}$$

$F^{(n)}(\omega)$ is equivalent to a cumulative oscillator strength for the continuum range. Its differentiation yields an nth order approximate density function $\tilde{f}(\omega)$, known as Stieltjes density. This differentiation can be done in many ways. According to one of the most common recipes, the continuum oscillator strength density is computed pointwise (i.e., numerically) as the Stieltjes derivative

$$\tilde{f}(\omega) = \frac{dF^{(n)}}{d\omega^{(n)}} = \tfrac{1}{2} \frac{f_{i+1}^{(n)} + f_i^{(n)}}{\omega_{i+1}^{(n)} - \omega_i^{(n)}} \tag{9}$$

at energy

$$\omega = \tfrac{1}{2}\left(\omega_{i+1}^{(n)} + \omega_i^{(n)}\right). \tag{10}$$

Finally, the detachment (or ionization) cross section is calculated from Eq. (1) employing $\tilde{f}(\omega)$, so that each order n gives $n-1$ points on the cross-section curve. These could be interpolated to yield a continuous curve. In the following, for a chosen value of r, we compute sequences of n principal pairs of frequencies and strengths (abscissae and weights), with $n = 2, \ldots, r$. Each sequence yields $n-1$ energies and cross-section points, which we then plot as separate points.

Here, we obtain the primitive spectrum from the poles and residues of the CC linear response function (diagonal component) expressed in the basis of left and right eigenvectors of a (truncated) tridiagonal representation of the CC Jacobian generated by an asymmetric Lanczos procedure.[25,26] For an operator (component) X,

$$\langle\langle X;X\rangle\rangle_{\omega}^{(J)} = u^X v^X \sum_j \frac{2\omega_j^{(J)} L_{j1}^{(J)} R_{1j}^{(J)}}{\left(\omega-\omega_j^{(J)}\right)\left(\omega+\omega_j^{(J)}\right)} - (v^X)^2 \sum_{jl} \frac{\left[\mathcal{F}_{jl} L_{j1}^{(J)} L_{l1}^{(J)}\right]}{\left(\omega-\omega_j^{(J)}\right)\left(\omega+\omega_l^{(J)}\right)}. \quad (11)$$

Above, $\boldsymbol{L}_j^{(J)}$ and $\boldsymbol{R}_j^{(J)}$ are left and right eigenvectors, with eigenvalue $\omega_j^{(J)}$, obtained diagonalizing the (approximate) tridiagonal representation $\mathbf{T}^{(J)}$ of the CC Jacobian matrix $\mathbf{A}$ generated via the Lanczos algorithm, and $\mathcal{F}_{jl} = \sum_{\mu,\nu,m,n} \mathrm{F}_{\mu\nu} Q_{\mu m} Q_{\nu n} R_{mj}^{(J)} R_{nl}^{(J)}$, with $Q_{\mu m}$ indicating the elements of the $\mathbf{Q}$ matrix used to generate $\mathbf{T}^{(J)}$, and $\mathrm{F}_{\mu\nu}$ the elements of the CC $\mathbf{F}$ matrix, see Refs. 26 and 27 for details. The superscript (J) is used to indicate that the tridiagonal representation $\mathbf{T}^{(J)}$ is truncated at dimension J (commonly referred to as chain length), which is significantly smaller than the full dimension of the excitation space. Roman summation indices run on the truncated space dimension J, whereas Greek indices are the conventional CC excitation level indices in the full excitation space.

The diagonal expression in Eq. (11) is obtained under the assumption that bi-orthogonalized CC right-hand-side vectors[26,27] $\boldsymbol{\eta}^X$ and $\boldsymbol{\xi}^X$ are used as starting vectors in the Lanczos chain procedure

$$\mathbf{q}_1 = \frac{\boldsymbol{\xi}^X}{v^X}; \qquad v^X = ||\boldsymbol{\xi}^X||, \quad (12)$$

$$\mathbf{p}_1^T = \frac{\boldsymbol{\eta}^X}{u^X}; \qquad u^X = \frac{\boldsymbol{\eta}^X \boldsymbol{\xi}^X}{v^X} \quad (13)$$

with the factors u^X and v^X as norms of such vectors.

The oscillator strengths f_i of the individual excitations $(0 \to j)$ in the Lanczos primitive pseudo-spectrum are computed from the residues of the above linear response function, i.e., for the X Cartesian component of the electric dipole moment operator

$$f_i^{XX} = \frac{2}{3}\omega_i \lim_{\omega\to\omega_i} (\omega-\omega_i)\langle\langle X;X\rangle\rangle_{\omega} = \frac{2}{3}\omega_i^{(J)} \left\{ u^X v^X L_{i1}^{(J)} R_{1i}^{(J)} - (v^X)^2 \sum_l \frac{\mathcal{F}_{li} L_{i1}^{(J)} L_{l1}^{(J)}}{\left(\omega_i^{(J)}+\omega_l^{(J)}\right)} \right\}. \quad (14)$$

Increasing the chain-length value, an increasing amount of pseudo-eigenvectors will converge to true accurate eigenvectors, allowing standard CC calculations of transition properties. We refer to Refs. 25 and 26 for additional details on the Lanczos procedure employed here.

III. COMPUTATIONAL DETAILS

Calculations of the CC pseudo-spectra have been performed at the CCS, CC2, and CCSD level using the Dalton program package,[28,29] which has been interfaced to our own Stieltjes imaging procedure.[11] Since H^- is a two-electron system, the CCSD results correspond to full-configuration interaction (FCI) results.

For all systems, correlation consistent basis sets of Dunning and co-workers have been employed, specifically singly (aug-), doubly (d-aug-), and triply (t-aug) augmented valence and core-valence sets cc-p(C)VXZ with X=D, T, Q, depending on the system. As the Stieltjes procedure is extremely sensitive to the description of the continuum, additional continuum-like Gaussian basis functions, constructed using the expression and parameters given by Kaufmann and co-workers,[30] were added, which were centered in the center of mass. Either sets of s and p or sets of s, p, and d continuum-like functions, with quantum number n from 1 to 20, or from 1 to 25 were employed, depending on the specific case at hand. They are labeled *nsnpnd* below. All electrons were correlated in all calculations. The experimental equilibrium geometry was used for OH^-.[31]

All plots have been generated using Matplotlib.[32] The experimental and computational data points we compare with have been digitized using WebPlotDigitizer.[33]

IV. DISCUSSION OF RESULTS

As previously pointed out in the literature,[11,14,20,34,35] the Stieltjes imaging procedure tends to become numerically unstable if the spectral moments used are not highly converged (accurate). The instability plagues mostly the points of the lowest and the highest orders and it manifests itself in rather scattered cross section points and/or odd features in the cross-section profiles. It has therefore been suggested in the literature to only retain orders in between 6 and 12. Many of our results, however, appear to be remarkably stable in this respect, so even the low and high orders are converged. We showcase this by presenting, for selected cases, both the plots were all points obtained in the Stieltjes procedure (orders from 2 to 20) are included, and "filtered" plots where the orders yielding clearly divergent points were removed, one next to the other. Which points were removed depends on the system considered and can be seen in the legend of the plots. Roughly, for all of the systems, the orders in between 6 and 12 yield stable results. As also done in our previous study,[11] we have chosen to plot the individual points from each Stieltjes order, instead of interpolating the collective series of points belonging to the "stable" orders, again to emphasize the essence of the Stieltjes imaging procedure.

One crucial point in the assessment of the accuracy of our procedure is the choice of basis set, which must contain some

of the physical characteristics of the continuum wavefunction, along with polarization and diffuse functions for a reasonable description of the bound discrete excitations. As already mentioned, inclusion of sets of "continuum-like" Gaussian basis functions of Kaufmann *et al.*[30] is a *sine-qua-non* condition to generate sufficiently accurate spectral moments on which the Stieltjes procedure can be applied with confidence. For all systems we tested different combinations of singly, doubly, and triply augmented Dunning sets and continuum-like functions. All the resulting plots are collected in the supplementary material,[36] whereas only the results of selected sets will be discussed in the following.

Another factor that may affect the quality of the results is the choice of length of the Lanczos chain, i.e., the dimension of the truncated representation of the CC Jacobian used to generate the pseudo-spectrum. We have therefore performed, for each system in selected basis sets an analysis of the convergence of the results at varying chain lengths, $J = 500$, $J = 2000$, and $J = 3000$. In all cases, the results were basically converged already with a chain length of 500, but we have chosen to report the results for the largest chain length, $J = 3000$, used. Note that for the two-electron system H^- and for all the CCS calculations, the dimension of the full excitation space was always used.

A. Hydride anion, H^-

The FCI results of H^- are presented in Fig. 1, and compared against calculations by Wishart,[37] by Oana and Krylov,[38] and by Venuti and Decleva,[39] and versus the experimental points of Smith and Burch.[40] The latter, reported in Table I of the original paper as relative cross-section points,[40] are here scaled such that the maximum of the experimental cross section coincides with the maximum of Wishart's cross section. After testing different basis sets from the Dunning series (see the supplementary material[36]), we settled for the t-aug-cc-pVQZ+25*s*25*p*25*d* basis set as "best" basis set for this system.

The main feature of the H^- cross section is a large (non-resonant) peak centered at around 1.5 eV, with a maximum height of approximately 40 Mb. Then, at around 11 eV, there is a series of auto-detaching resonances, and precisely two very sharp ones at 10.92 eV and 10.95 eV and a broader one at 10.98 eV, which are of interest in cosmology.[41] This area is marked with a vertical dashed line in Fig. 1. A detailed discussion of experimental and theoretical results for the autoionizing resonances can be found in Refs. 7 and 41.

As it can be appreciated from Fig. 1, and from the detail in the region 0.5–3.5 eV shown in Fig. 2, the non-resonant peak is well reproduced by our FCI calculation. Moreover, even if sharp and narrow auto-ionizing resonances are considered to be extremely challenging (if not impossible) to obtain with the Stieltjes procedure,[14] we observe that some sharp features seem to emerge from the cross-section points of the higher Stieltjes orders (corresponding well to the peak obtained by Venuti and Decleva,[39]) accompanied by irregularities in the slope of the curve beginning roughly at 11 eV. Our "filtered" data, see right panel of Figs. 1 and 2, fit perfectly to the calculations of Wishart[37] and of Venuti and Decleva,[39] which we treat as the best reference results here, up to around 6 eV, after which our tail decays more slowly than these curves.

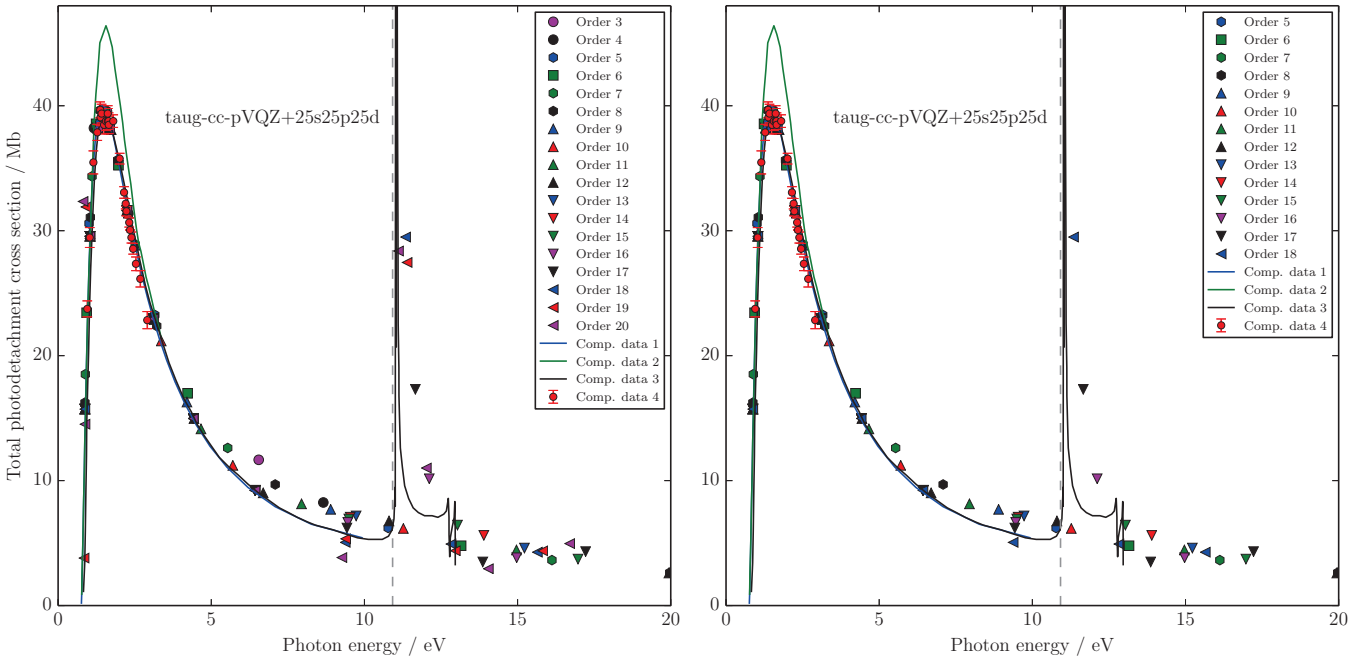

FIG. 1. Hydride anion H^-. Photodetachment cross section points from Stieltjes imaging of FCI pseudo-spectra in the t-aug-cc-pVQZ+25*s*25*p*25*d* basis set. The cross section points from all Stieltjes orders up to 20 are shown on the left panel, whereas the points for orders from 5 to 15 only are shown on the right panel. "Comp. data 1" are calculations by Wishart.[37] "Comp. data 2" are the EOM-CCSD Dyson results of Oana and Krylov in the 6-311G(4+)(3*pd*) basis set.[38] "Comp. data 3" are the general Configuration Interaction/B-spline results by Venuti and Decleva.[39] "Comp. data 4" are experimental points by Smith and Burch.[40] The vertical dashed line indicates the onset of the resonances at around 11 eV. The chain length J was equal to the full dimension of the excitation space in the given basis set.

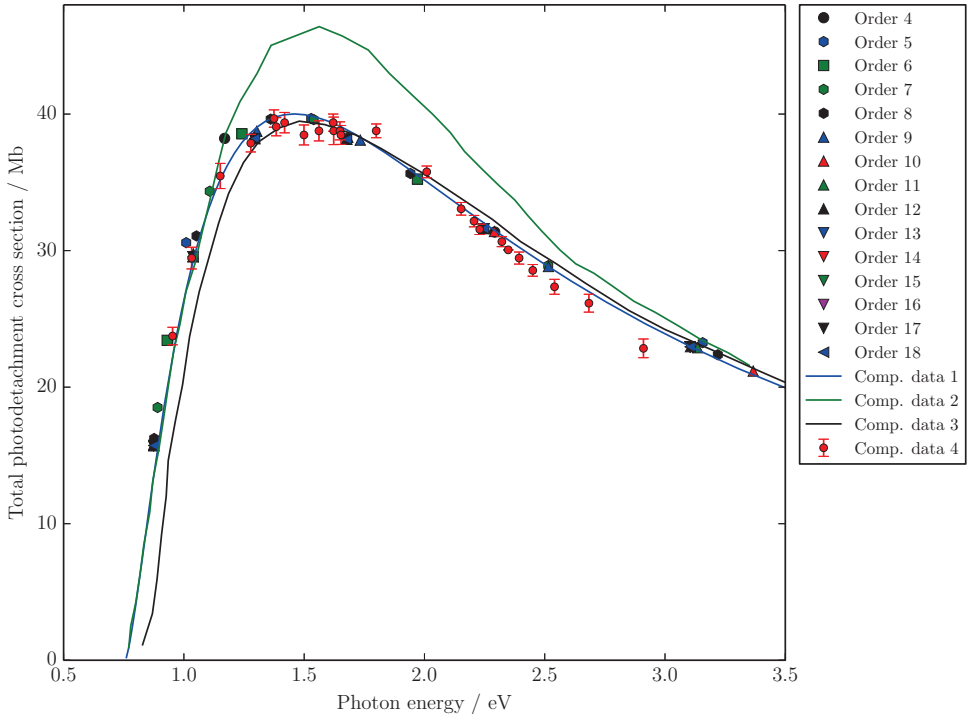

FIG. 2. Hydride anion H^-. Detail of the FCI results obtained with the t-aug-cc-pVQZ+2*5s*2*5p*2*5d* basis set in the energy region between 0.5 and 3.5 eV. "Comp. data 1" are calculations by Wishart.[37] "Comp. data 2" are the EOM-CCSD Dyson results of Oana and Krylov in the 6-311G(4+)(3*pd*) basis set.[38] "Comp. data 3" are the general Configuration Interaction/B-spline results by Venuti and Decleva.[39] "Comp. data 4" are experimental points by Smith and Burch.[40]

On the other hand, the cross-section profile obtained at the EOM-CCSD level by Oana and Krylov,[38] employing Dyson orbitals and a plane-wave description of the detached electron is overestimated and it peaks at slightly higher energy than experiment. The remarkable difference between the EOM results of Ref. 38 and ours results could be partly ascribed to the uncorrelated treatment of the ejected electron in Ref. 38, and partly to limitations in the description of the continuum orbital. Other studies on the detachment of H^- are those of Tang *et al.*,[42] and of Sadeghpour *et al.*[43]

The results obtained with the CCS and CC2 approximations, see Fig. 3, yield cross-section curves that in both

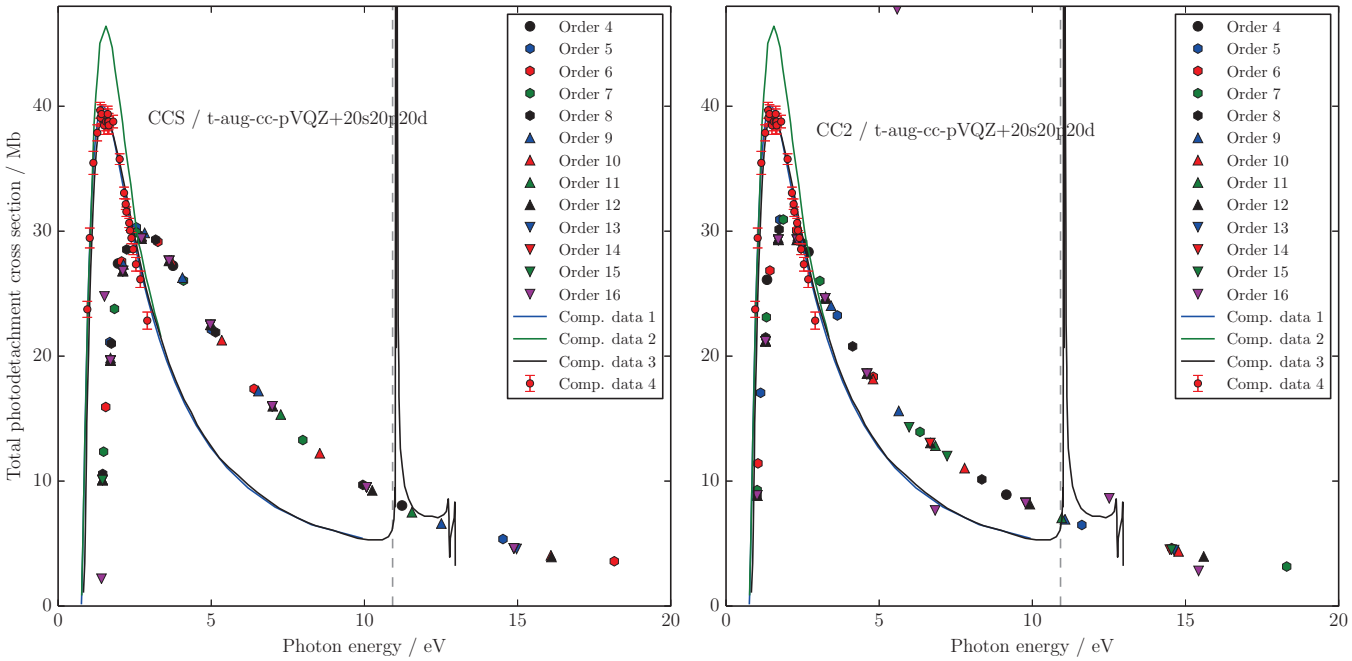

FIG. 3. Hydride anion H^-. Photodetachment cross section points from Stieltjes imaging of CCS (left) and CC2 (right) pseudo-spectra in the t-aug-cc-pVQZ+20*s*20*p*20*d* basis set. "Comp. data 1" are calculations by Wishart.[37] "Comp. data 2" are the EOM-CCSD Dyson results of Oana and Krylov in the 6-311G(4+)(3*pd*) basis set.[38] "Comp. data 3" are the general Configuration Interaction/B-spline results by Venuti and Decleva.[39] "Comp. data 4" are experimental points by Smith and Burch.[40]

cases are too broad and too low, as well as shifted at higher energies.

B. Lithium anion, Li^-

The CCSD results for Li^-, obtained both in the aug-cc-pVDZ+25*s*25*p*25*d* and in the t-aug-cc-pCVQZ+25*s*25*p*25*d* basis sets, are shown in Fig. 4 together with the experimental results of Kaiser *et al.*,[44] of Bae and Peterson,[9] of Dellwo *et al.*,[45] the Multi-Configurational Tamm-Dancoff (MCTD) results by Jose *et al.*,[8] the unscaled EOM-CCSD Dyson cross-section profile of Oana and Krylov in the 6-311G(4+)(3*pd*) basis set,[38] the Stieltjes CCSDT1aPPA curve of Canuto *et al.*,[46] and with the cross-section obtained by Carravetta *et al.*[10] applying Stieltjes imaging to Multiconfigurational Linear Response spectral moments. The absolute photodetachment cross sections obtained with other basis sets are shown in the supplementary material. Note that, as for H^-, Li^- has no excitation in the primitive spectrum of bound character.

The cross section spectrum of Li^- is characterized by two main features: a first, broad, band at around 1 eV (2*s* threshold), and a second, sharp cusp-like peak at around 2.5 eV (aka 2*p* threshold, due to the shake-up process after detachment that leaves the Li atom in a ^2P state). Compared to the experimental data of Ref. 44 (which according to the authors could be in error by as much as 30%), our CCSD results reproduce reasonably well both the height of the broad peak and the position of both peaks. Actually, the experimental data around 1.0–2.0 eV exhibit some additional structure which is partly reflected by some degree of clustering of our Stieltjes points, although no evidence of resonances has been detected in previous calculations below the 2*p* threshold. Remarkably, despite the fact that in the Stieltjes imaging procedure very sharp features are in general "smoothened" and tend to disappear, in this case, as also seen for H^-, the method and basis sets used yield spectral moments that are sufficiently accurate to reproduce the sharp resonance at around 2.5 eV, especially when the points from the higher Stieltjes orders are retained. We present results obtained with two different basis sets to show that in the smaller basis set there is an artifact feature, appearing as a broad peak, at around 3 eV, which disappears completely when the larger basis set, allowing better convergence for the spectral moments, is employed. This illustrates an inherent risk when using Stieltjes imaging that non-existent structures may show up with an inadequate model/basis set.

As for the theoretical results reported earlier in the literature,[8–10,44,46–51] the MCTD results of Ref. 8 underestimate the main peak and overestimate the cross section values in the region preceding the sharp resonance compared to experiment.[44] On the other hand, Relativistic Random-Phase-Approximation calculations reported therein[8] do not reproduce the 2*p*-cusp at all. The yet earlier *R*-matrix calculations by Ramsbottom *et al.*[52] overestimate the values of the cross section in this region as well, and so do the *K*-matrix results of Moccia and Spizzo[49] and Configuration-Interaction/close-coupling[53] results of Moores and Norcross. The CCSDT1aPPA+Stieltjes curve of Canuto *et al.*[46] is shifted in energy and lower than both our and the experimental points. The MCSCF+Stieltjes results of Carravetta *et al.*[10] do quite well in reproducing the broad peak above the 2*s* threshold, and lie very close to our results. Finally, the

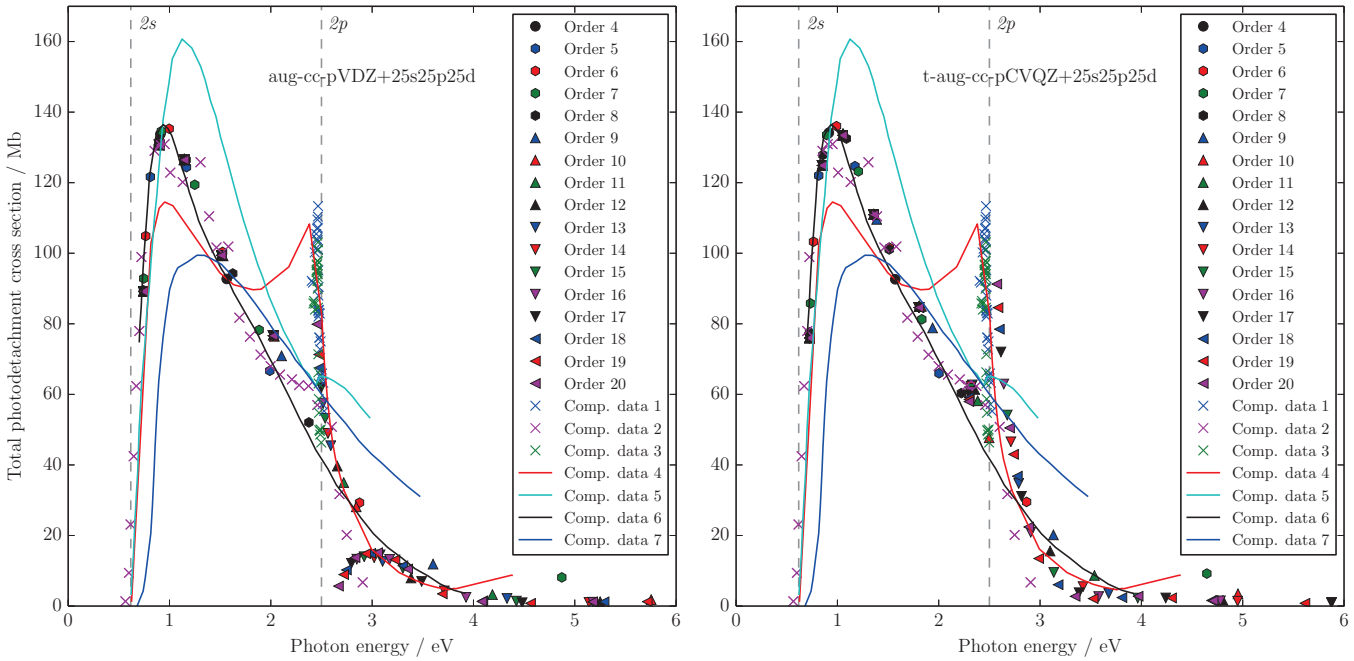

FIG. 4. Lithium anion Li^-. Photodetachment cross section points from Stieltjes imaging of Lanczos CCSD pseudo-spectra with chain length $J = 3000$. "Comp. data 1" indicate the experiment by Bae and Peterson.[9] "Comp. data 2" are the experiment by Kaiser *et al.*[44] "Comp. data 3" are the experiment by Dellwo *et al.*[45] "Comp. data 4" are MCTD calculations by Jose *et al.*,[8] whereas "Comp. data 5" are the unscaled EOM-CCSD Dyson data of Oana and Krylov in the 6-311G(4+)(3*pd*) basis set.[38] "Comp. data 6" are the MCLR/Stieltjes cross-section by Carravetta *et al.*,[10] and "Comp. data 7" are the CCSDT1aPPA/Stieltjes cross section of Canuto *et al.*[46] Vertical dashed lines indicate the 2*s* and 2*p* thresholds.

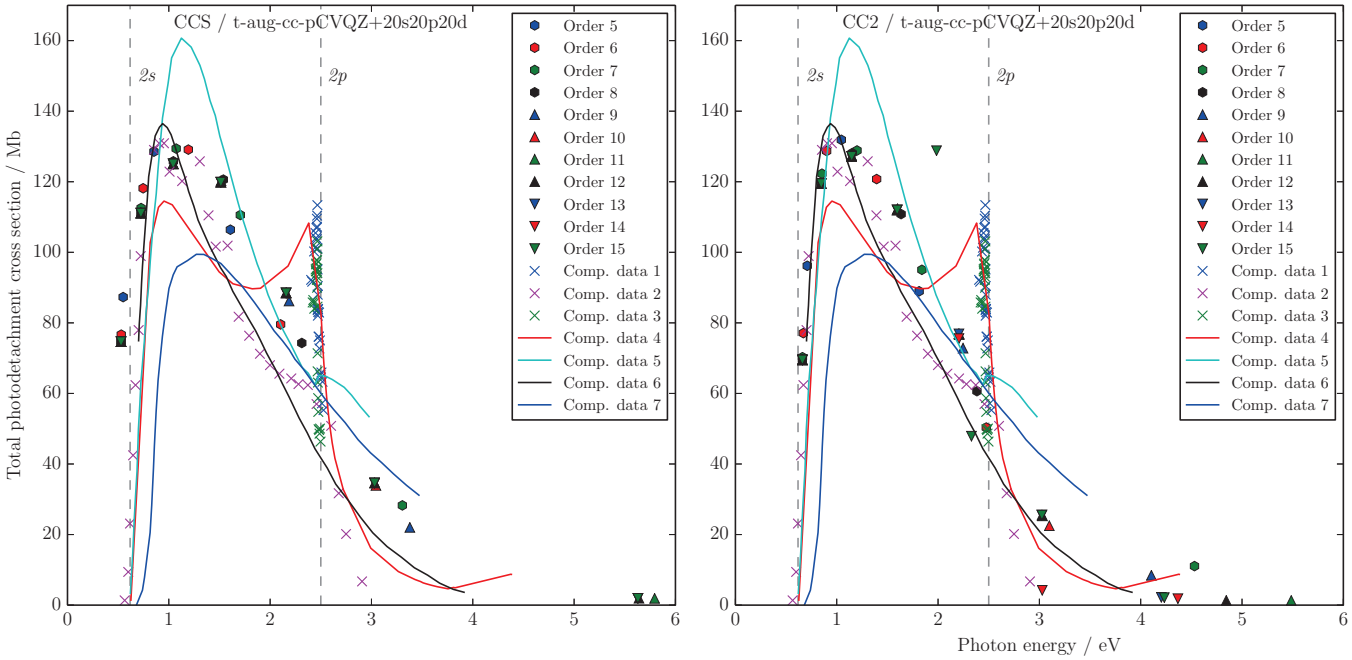

FIG. 5. Lithium anion Li^-. Photodetachment cross section points from Stieltjes imaging of Lanczos CCS (left) and CC2 (right) pseudo-spectra. "Comp. data 1" stand for the experiment by Bae and Peterson.[9] "Comp. data 2" are the experiment by Kaiser *et al.*[44] "Comp. data 3" are the experiment by Dellwo *et al.*[45] "Comp. data 4" are MCTD calculations by Jose *et al.*[8] "Comp. data 5" are the unscaled EOM-CCSD Dyson data of Oana and Krylov in the 6-311G(4+)(3pd) basis-set,[38] "Comp. data 6" are the MCLR/Stieltjes cross-section by Carravetta *et al.*,[10] and "Comp. data 7" are the Stieltjes CCSDT1aPPA cross section of Canuto *et al.*[46] Vertical dashed lines indicate the 2*s* and 2*p* thresholds.

(unscaled) cross-section profile obtained by Oana and Krylov using the Dyson-orbital EOM-CCSD approach[38] significantly overestimates the first peak, it is shifted on the energy axis, and it does not reproduce the fast drop (the cusp) after 2.5 eV.

To conclude this section, the cross-sections points obtained from the CCS and CC2 pseudo-spectra, shown in Fig. 5, are rather scattered, do not seem to reproduce the cusp in any conclusive manner, and deviate from the experimental curve in the region between the two main peaks. The rising edge of the main peak at around 1 eV, however, is reasonably well-reproduced, in particular at the CC2 level.

C. Sodium anion, Na^-

Our CCSD results for Na^-, obtained with the aug-cc-pCVTZ+20*s*20*p*20*d* basis set, are presented in Fig. 6. They are compared with the *R*-matrix calculations by Liu and Starace,[54] with the experimental data by Kaiser *et al.*,[44] with the Configuration-Interaction/close-coupling curve by Moores and Norcross,[53] and with the MCTD curve by José *et al.*[8]

The photodetachment cross section for Na^- yielded by the various methods is qualitatively very similar to that of Li^-, with a main broad peak at around 1 eV and a cusp-like peak at around 2.5 eV. According to the authors,[44] an error of about 30% error on the absolute values has to be attributed to the experimental data. It is remarkable that even if the same error could affect the Li^- cross section, the disagreement between theoretical and experimental cross sections is more pronounced for the Na^- anion. In view of our new results as well as the previous theoretical results, we believe that a normalization error by about a factor of 2 is affecting the experimental results of Na^-.

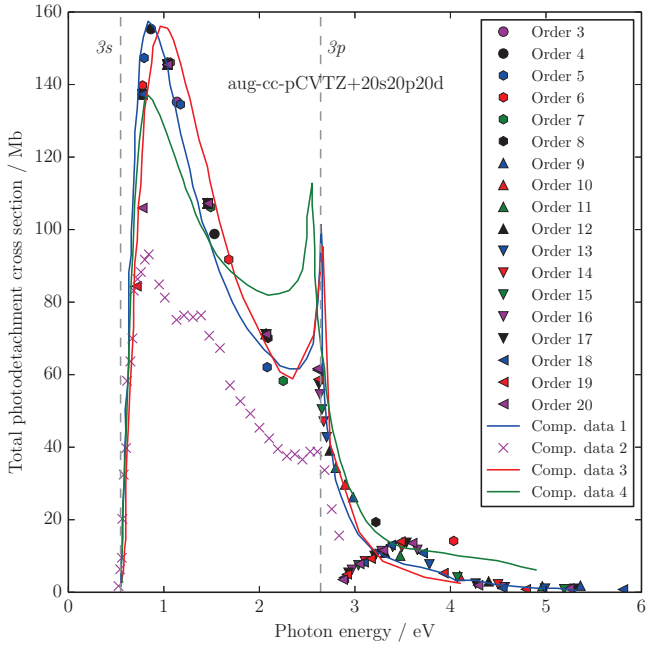

FIG. 6. Sodium anion, Na^-. Photodetachment cross section points from Stieltjes imaging of Lanczos CCSD pseudo-spectra in the aug-cc-pCVTZ+20*s*20*p*20*d* basis set and chain length $J = 3000$. "Comp. data 1" are *R*-matrix calculations by Liu and Starace.[54] "Comp. data 2" are experimental points by Kaiser *et al.*[44] "Comp. data 3" are calculations by Moores and Norcross.[53] "Comp. data 4" are MCTD calculations (in the length gauge) by Jose *et al.*[8]

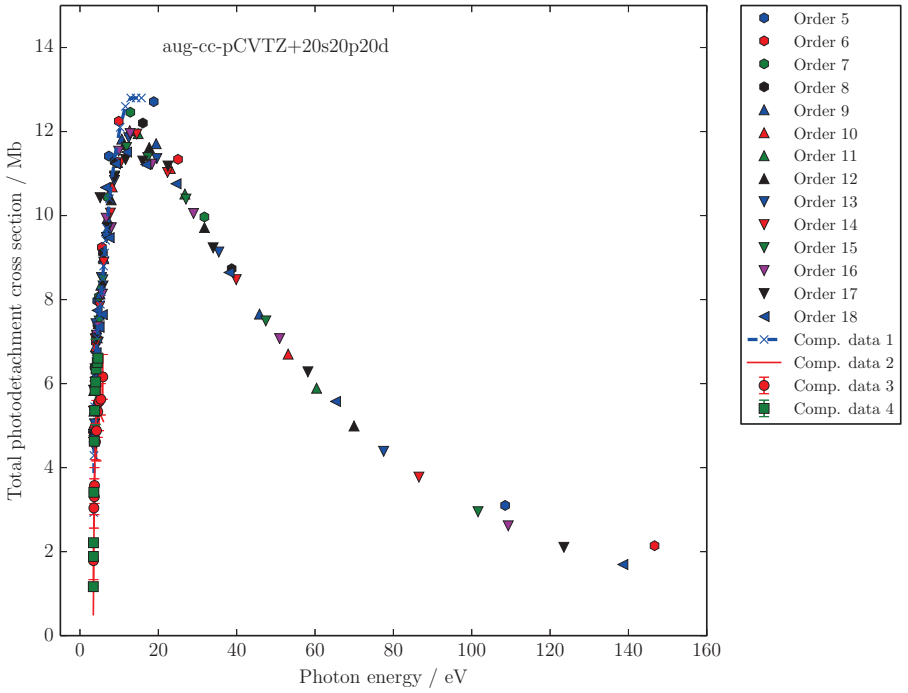

FIG. 7. Fluoride anion, F^-. Photodetachment cross section points from Stieltjes imaging of Lanczos CCSD pseudo-spectra in the aug-cc-pCVTZ+20*s*20*p*20*d* basis set and chain length $J = 3000$. "Comp. data 1" are calculations by Robinson and Geltman.[56] "Comp. data 2" is the EOM-CCSD Dyson cross-section curve calculated by Oana and Krylov.[38] "Comp. data 3" are experimental points from Mandl.[55] "Comp. data 4" are experimental points from Vacquié *et al.*[57]

As it can be seen from additional data in the supplementary material, in order to reproduce the cusp, the use of a core-valence basis set was necessary. The Stieltjes points obtained are rather scarce, but they match the previous results well. Similar to what was observed for Li^-, the peak emerging between 3 and 4 eV is probably an artifact, but larger basis set were not used because they were computationally too demanding. The *R*-matrix calculations by Liu and Starace[54] correspond to our results best.

D. Fluoride anion, F^-

The CCSD photodetachment cross section obtained for the fluoride anion in the aug-cc-pCVTZ+20s20p20d basis set and chain length $J = 3000$ is presented in Fig 7. It is compared with the experimental results by Mandl,[55] the theoretical results by Robinson and Geltman,[56] the measurements of Vacquie *et al.*,[57] and the EOM-CCSD Dyson cross-section profile by Oana and Krylov (in the 6-311G(3+)(3*df*) basis).[38]

The overall shape of the F^- cross-section resembles the photoionization cross section of the isoelectronic neon atom, even though displaced. There is one peak at around 20 eV, quickly descending to lower values. To the best of our knowledge, there are no sufficient experimental data in the literature to compare the entire cross section profile. The experimental data available from Mandl[55] only cover the frequency range 3.4–5.9 eV, and those from Vacquie *et al.*[57] fall in between 3.4 and 4.5 eV. Oana and Krylov also limit themselves to the experimental range 3.4–5.9 eV. The calculations by Robinson and Geltman[56] cover a wider range from 3.4 to 12.25 eV.

A magnification of the energy region between 3 and 12 eV in Fig. 8 shows in better detail how our results compare with the two sets of experimental and computational data. Our cross section points closely follow the cross section points obtained by Robinson and Geltman,[56] even though our maximum is lower than theirs. Comparing with the two sets of experimental data, our points are well within the experimental error bars of Vaquié *et al.*,[57] whereas they fall higher than

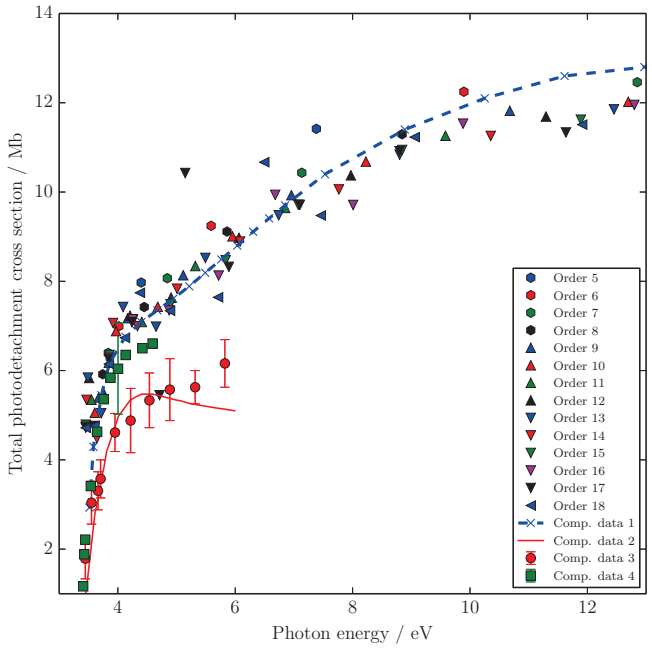

FIG. 8. Fluoride anion, F^-. Magnification of the photodetachment cross section between 3 and 13 eV. "Comp. data 1" are calculations by Robinson and Geltman.[56] "Comp. data 2" are the EOM-CCSD Dyson cross-section curve calculated by Oana and Krylov.[38] "Comp. data 3" are experimental points from Mandl.[55] "Comp. data 4" are experimental points from Vacquié *et al.*[57]

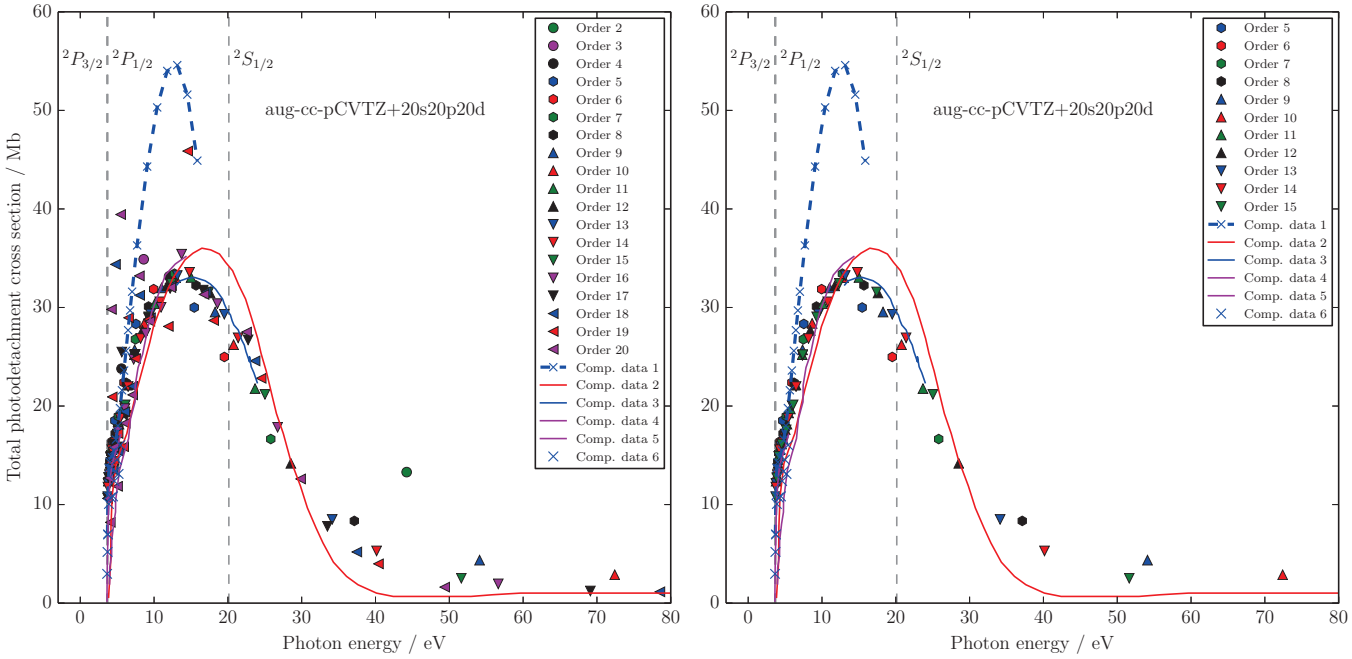

FIG. 9. Chloride anion, Cl^-. Photodetachment cross section points from Stieltjes imaging of Lanczos CCSD pseudo-spectra in the aug-cc-pCVTZ+20*s*20*p*20*d* basis set and chain length $J = 3000$. "Comp. data 1" are calculations by Robinson and Geltman[56] "Comp. data 2" are RRPA calculations of the σ_{3p} partial cross section by Radojevic *et al.*[58] "Comp. data 3" are velocity MBPT calculations calculations of the σ_{3p} partial cross section by Radojevic *et al.*[58] "Comp. data 4" are length MBPT calculations calculations of the σ_{3p} partial cross section by Radojevic *et al.*[58] "Comp. data 5" are RRPA calculations by Kutzner *et al.*[59] "Comp. data 6" are experimental points by Mandl *et al.*[60]

those of Mandl.[55] A remarkable difference is also observed in the comparison to Oana and Krylov's cross-section profile.

E. Chloride anion, Cl^-

The CCSD photodetachment cross section of Cl^- obtained with the aug-cc-pCVTZ+20*s*20*p*20*d* basis set and chain length $J = 3000$ is presented in Fig. 9.

The profile is rather similar to the one of the isoelectronic argon atom if one disregards the auto-ionizing pit in the Ar cross section.[11] As for Na^-, also for this system the experimental data[60] are scarce and it is possible to compare results only in the narrow region between 3.5 and 5.6 eV, see Fig. 10 for magnification of this region including both the experimental results by Mandl *et al.*[60] and the Relativistic Random Phase Approximation (RRPA) calculations by Kutzner *et al.*[59] Our results align above the experimental data.[60] The computational results of Robinson and Geltman[56] are reasonably close to our results and both fall just outside the experimental error bars in the region 3.5–5.5 eV, but after 5.5 eV their cross section grows much more rapidly than ours and peaks at 55 Mb, whereas our maximum is below 35 Mb. The cross section profile sketched by our Stieltjes points also seems to decay more slowly than the partial σ_{3p} cross section (which is the dominant contribution to the total cross section, σ_{tot}) computed by Radojević *et al.*[58]

F. Hydroxide ion, OH^-

Our CCSD results for hydroxide anion OH^- are shown in Fig. 11. They were obtained in the aug-cc-pCVTZ+20*s*20*p*20*d* basis set with chain-length $J = 3000$. We compare them with experimental data measured by Branscomb,[61] by Lee and Smith,[62] and with the EOM-CCSD Dyson calculations by Oana and Krylov.[38] The profile

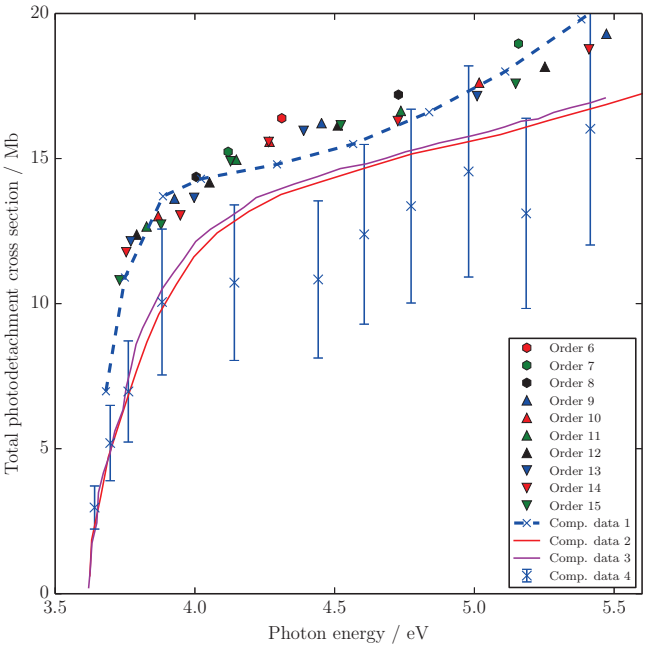

FIG. 10. Chloride anion, Cl^-. Detail of the photodetachment cross section in the energy region 3.5–5.6 eV. "Comp. data 1" are calculations by Robinson and Geltman.[56] "Comp. data 2" are RRPA calculations of the σ_{3p} partial cross section by Radojevic *et al.*[58] "Comp. data 3" are calculations by Kutzner *et al.*[59] "Comp. data 4" are experimental points by Mandl *et al.*[60]

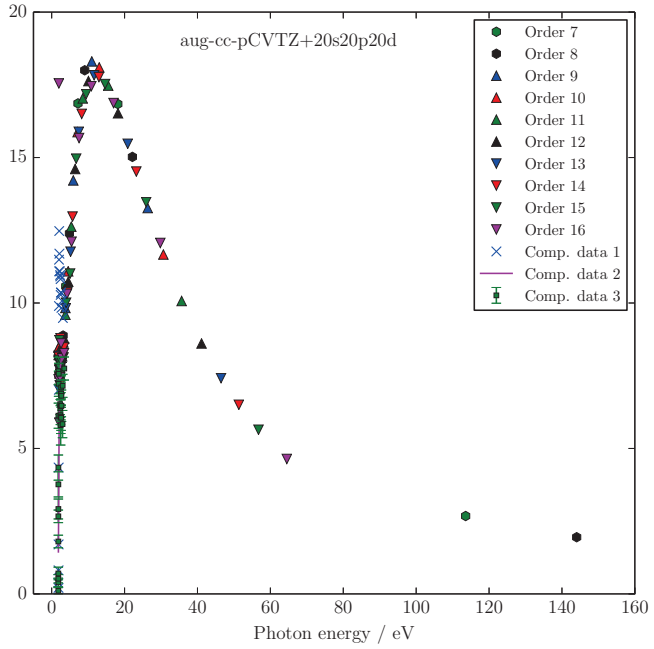

FIG. 11. Hydroxide anion, OH^-. Photodetachment cross section points obtained at the CCSD level in the aug-cc-pCVTZ+20*s*20*p*20*d* basis set and chain-length $J = 3000$. "Comp. data 1" are experiment points by Branscomb.[61] "Comp. data 2" are the original (unscaled) EOM-CCSD Dyson cross section curve from Oana and Krylov.[38] "Comp. data 3" are experimental points by Lee and Smith.[62]

features one broad peak at around 20 eV and the typical ionization decay, with no apparent coupling to other channels in the investigated region.

As the previous results, both experimental[61–63] and computational,[38] cover only a small region of low photon energies, we also report, in Fig. 12, a detail of the cross section plot between 1 and 4 eV. Despite being slightly scattered, our CCSD results in this region fall in between the experimental data of Branscomb,[61] and those of Lee and Smith (measured in O_2).[62] Hlavenka *et al.*[63] conducted low-temperature measurements of the photodetachment cross sections of the OH^- anion and reported two temperature-averaged cross section values at 662 nm (≈1.873 eV) and 632.8 nm (≈1.962 eV) of $8.5(1)_{stat}(3)_{syst}$ Mb and $8.1(1)_{stat}(7)_{syst}$ Mb, respectively. The two results are also in line with our cross-section points. The agreement with the unscaled results of Oana and Krylov is also reasonable.

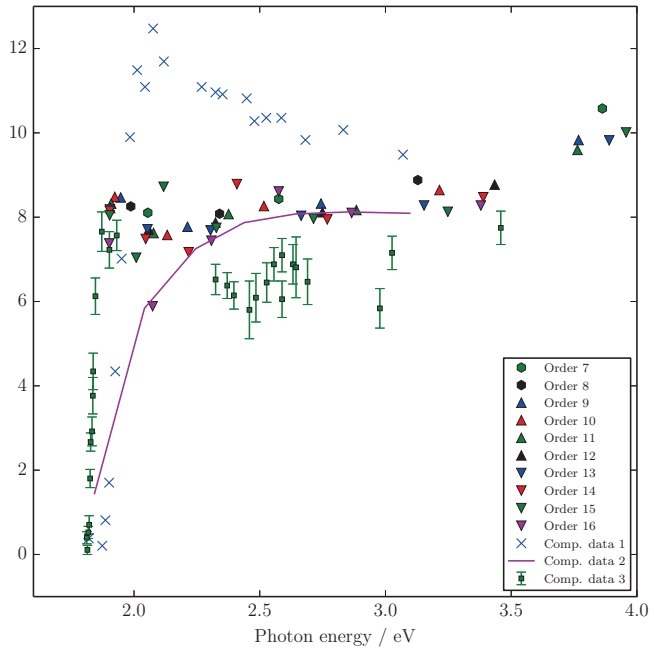

FIG. 12. Hydroxide anion, OH^-. Detail of the CCSD photodetachment cross section in the energy region 0.0–5.0 eV. "Comp. data 1" are experimental points by Branscomb.[61] "Comp. data 2" are the original (unscaled) EOM-CCSD Dyson cross section curve from Oana and Krylov.[38] "Comp. data 3" are experimental points by Lee and Smith.[62]

The CCS and CC2 results are reported in Figs. 13 and 14. Overall, the CCS cross section profile is shifted towards higher energy and peaks at higher values of the cross section, as also observed for H^-. The CC2 results display some remarkable anomalies: the onset of the profile (threshold) is at much lower energies than the experimental values, and two different curves appear to emerge from the different Stieltjes orders. The reason for such behaviour could not be ascertained.

V. CONCLUSIONS

We have presented the results of an *ab initio* investigation of the total photodetachment cross section profiles (in the region of ionization from valence orbitals) of selected (closed-shell) atomic and molecular ions, obtained applying Stieltjes imaging to coupled-cluster Lanczos pseudo-spectra.

Apart from isolated features over very small energy ranges, very few wide energy photodetachment cross sections are experimentally available, pointing out the importance of quantitative theoretical estimates on the absolute scale.

For the atomic ions, CCSD is found to yield cross-section profiles in good agreement with the available experimental data and the best theoretical results both with respect to the overall shape and the absolute scale, showcasing the importance of dynamical correlation contribution for a quantitative reproduction of total cross section values of negative ions. On the other hand, the CCS and CC2 methods, which we tested for H^-, Li^-, and OH^-, proved to be too inaccurate. For H^- they yield broader cross section profiles significantly shifted towards higher energies compared to the established reference values,[37,41] and for Li^- very scattered cross-section points. For the molecular anion OH^-, the CCS profile is shifted towards higher energies and cross-section values, whereas the CC2 results show anomalies whose origin remains unclear. The fact that the CC2 approach appears to work well for photoionization,[11] but not quite so for photodetachment, is intriguing, yet not entirely unexpected. In fact, it is reasonable to assume that the ground state of an anion is more correlated than the ground state of the corresponding neutral species. One can expect the importance of double excitations to grow in the anions compared to the neutral species, and therefore the intrinsic approximations in the CC2 approach to become a more severe limiting factor in the description of photodetachment than of photoionization.

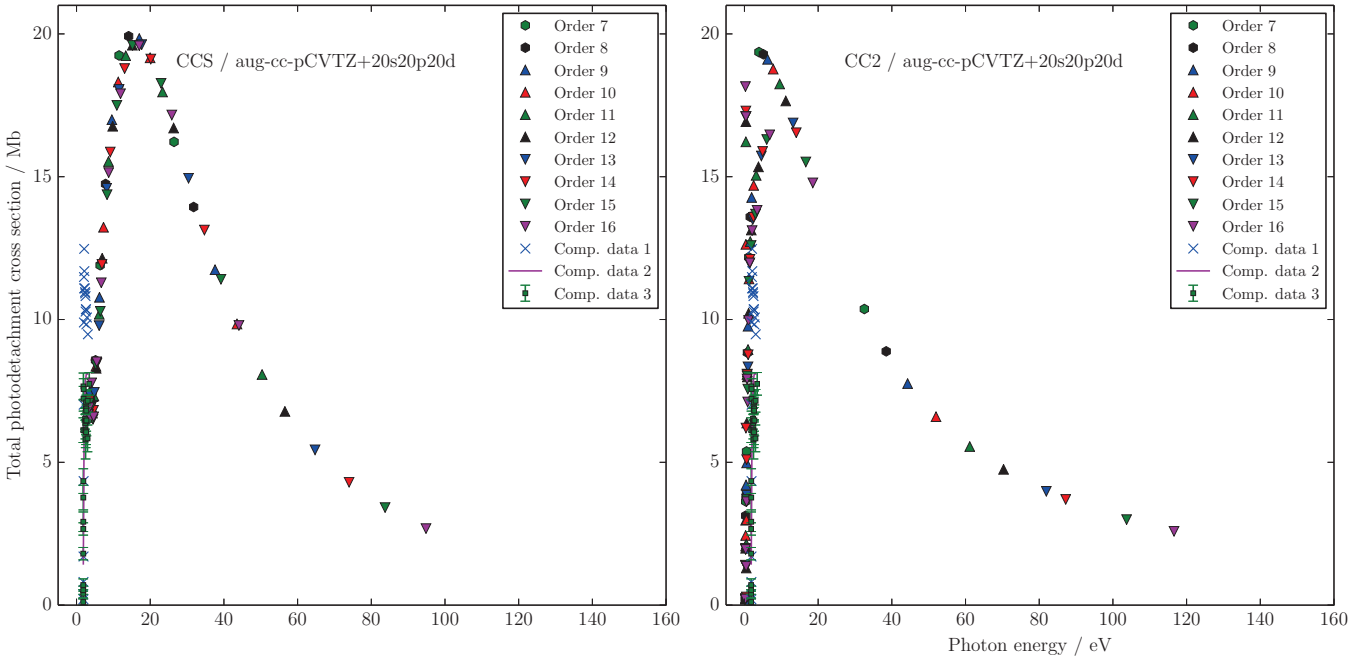

FIG. 13. Hydroxide anion, OH^-. Photodetachment cross section results obtained with the CCS and CC2 approximations. The chain length J in the case of the CCS is equal to the full dimension of the excitation space. For CC2, $J = 3000$. "Comp. data 1" are experimental points by Branscomb.[61] "Comp. data 2" are the original (unscaled) EOM-CCSD Dyson cross section curve from Oana and Krylov.[38] "Comp. data 3" are experimental points by Lee and Smith.[62]

In conclusion, we have shown that our approach can provide accurate results for photodetachment, and in particular absolute values of the total cross section in regions free from very sharp resonances. They compare very well with the most accurate results available, and can clearly distinguish between competing experimental or theoretical results, and in particular deficiencies in the absolute values of the former. They can be easily extended to more complex molecular systems, for which absolute data are needed but experimental values are missing or very difficult to obtain. Still further analysis of basis sets is needed to guarantee convergence, and some data processing to obtain smooth results.

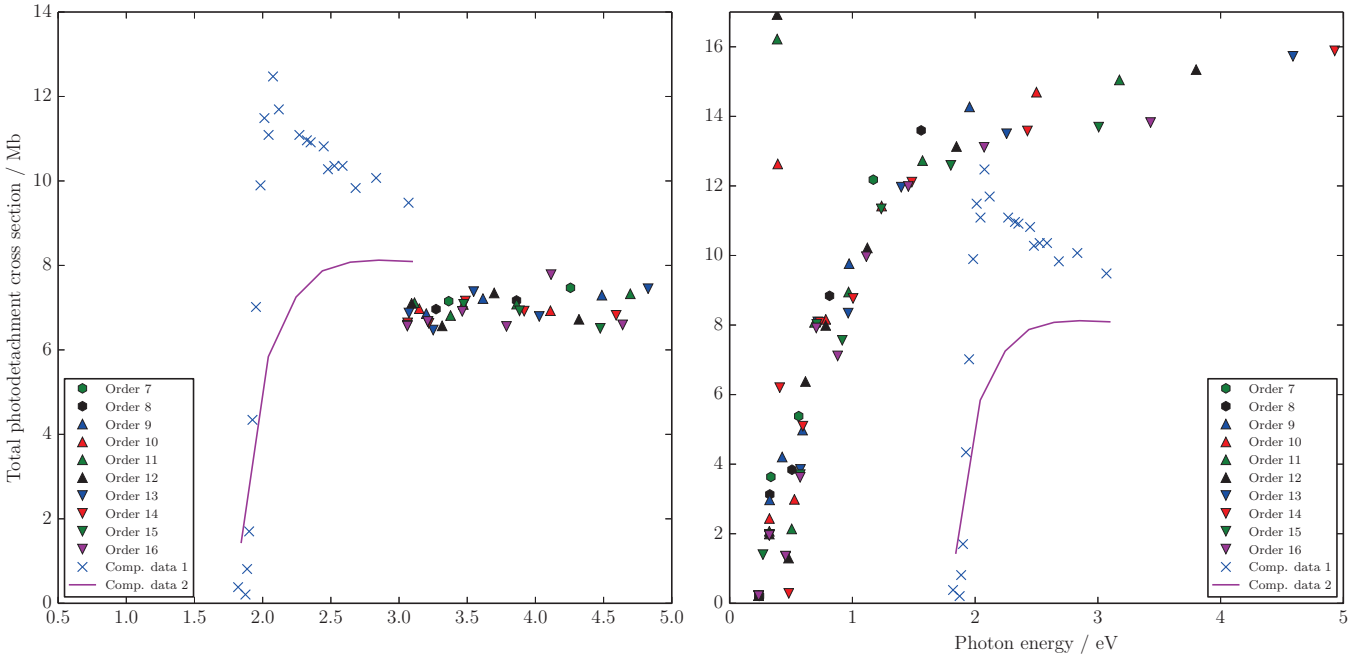

FIG. 14. Hydroxide anion, OH^-. Magnification of the CCS (left) and CC2 (right) photodetachment cross sections in the energy region 1.0–4.0 eV. "Comp. data 1" are experimental points by Branscomb.[61] "Comp. data 2" are the original (unscaled) EOM-CCSD Dyson cross section curve from Oana and Krylov.[38] "Comp. data 3" are experimental points by Lee and Smith.[62]

ACKNOWLEDGMENTS

We thank Dr. J. Jose for supplying us with the raw data of the investigation in Ref. 8. This work has been supported by the Italian PRIN2009 funding scheme (Project No. 2009C28YBF_001) and by the FP7-PEOPLE-2009-IEF funding scheme (S.C., Project No. 254326).

[1]The Opacity Project Team, in *The Opacity Project* (Institute of Physics Publishing, Bristol, 1995), Vol. **1**, pp. 1–29.
[2]M. J. Seaton, Mon. Not. R. Astron. **362**, L1 (2005).
[3]J. S. Hirsch, E. T. Kennedy, A. Neogi, J. T. Costello, P. Nocolosi, and L. Poletto, Rev. Sci. Instrum. **74**, 2992 (2003).
[4]R. P. Wayne, *Chemistry of Atmospheres, 3rd ed.* (Oxford University Press, New York, 2000).
[5]B. M. Smirnov, *Physics of Ionized Gases* (John Wiley and Sons, New York, 2001).
[6]T. Andersen, Phys. Rep. **394**, 157 (2004).
[7]P. Balling, H. Andersen, C. Brodie, U. Pedersen, V. Petrunin, M. Raarup, P. Steiner, and T. Andersen, Phys. Rev. A. **61**, 022702 (2000).
[8]J. Jose, G. B. Pradhan, V. Radojević, S. T. Manson, and P. C. Deshmukh, Phys. Rev. A. **83**, 053419 (2011).
[9]Y. K. Bae and J. R. Peterson, Phys. Rev. A. **32**, 1917 (1985).
[10]V. Carravetta, H. Ågren, H. Jensen, P. Jørgensen, and J. Olsen, J. Phys. B: At. Mol. Opt. Phys. **22**, 2133 (1989).
[11]J. Cukras, S. Coriani, P. Decleva, O. Christiansen, and P. Norman, J. Chem. Phys. **139**, 094103 (2013).
[12]P. W. Langhoff and C. Corcoran, J. Chem. Phys. **61**, 146 (1974).
[13]P. Langhoff, C. Corcoran, J. Sims, F. Weinhold, and R. Glover, Phys. Rev. A. **14**, 1042 (1976).
[14]F. Müller-Plathe, and G. H. Diercksen, "Molecular photoionisation cross sections by moment theory. An introduction," in *Electronic Structure of Atoms, Molecules and Solids, in Proceeding of the II Escola Brasileira de Estructure Eletronica, Olinda, Brazil, July 17–22, 1989*, edited by S. Canuto, J. D'Albuquerque e Castro, and F. J. Paixao, (Olinda, Brazil, 1990), pp. 1–29.
[15]V. Carravetta and H. Ågren, Phys. Rev. A. **35**, 1022 (1987).
[16]H. Ågren and V. Carravetta, J. Chem. Phys. **87**, 370 (1987).
[17]V. Carravetta and H. Ågren,; J. Phys. **C9**(48), 769 (1987).
[18]V. Carravetta, Y. Luo, and H. Ågren, Chem. Phys. **174**, 141 (1993).
[19]V. Averbukh and L. S. Cederbaum, J. Chem. Phys. **123**, 204107 (2005).
[20]K. Gokhberg, V. Vysotskiy, L. S. Cederbaum, L. Storchi, F. Tarantelli, and V. Averbukh, J. Chem. Phys. **130**, 064104 (2009).
[21]S. Kopelke, K. Gokhberg, V. Averbukh, F. Tarantelli, and L. S. Cederbaum, J. Chem. Phys. **134**, 094107 (2011).
[22]S. Kopelke, K. Gokhberg, L. S. Cederbaum, F. Tarantelli, and V. Averbukh, J. Chem. Phys. **134**, 024106 (2011).
[23]M. Ruberti, R. Yun, K. Gokhberg, S. Kopelke, L. S. Cederbaum, F. Tarantelli, and V. Averbukh,; J. Chem. Phys. **139**(14), 144107 (2013).
[24]M. Ruberti, R. Yun, K. Gokhberg, S. Kopelke, L. S. Cederbaum, F. Tarantelli, and V. Averbukh,; J. Chem. Phys. **140**(18), 184107 (2014).
[25]S. Coriani, O. Christiansen, T. Fransson, and P. Norman, Phys. Rev. A. **85**, 022507 (2012).
[26]S. Coriani, T. Fransson, O. Christiansen, and P. Norman, J. Chem. Theory Comput. **8**, 1616 (2012).
[27]O. Christiansen, C. Hättig, and P. Jørgensen, Int. J. Quantum Chem. **68**, 1 (1998).
[28]K. Aidas, C. Angeli, K. L. Bak, V. Bakken, R. Bast, L. Boman, O. Christiansen, R. Cimiraglia, S. Coriani, P. Dahle, E. Dalskov, U. Ekström, T. Enevoldsen, J. J. Eriksen, P. Ettenhuber, B. Fernández, L. Ferrighi, H. Fliegl, L. Frediani, K. Hald, A. Halkier, C. Hättig, H. Heiberg, T. Helgaker, A. C. Hennum, H. Hettema, E. Hjertenaes, S. Høst, I.-M. Høyvik, M. F. Iozzi, B. Jansík, H. Jensen, D. Jonsson, P. Jørgensen, J. Kauczor, S. Kirpekar, T. Kjaergaard, W. Klopper, S. Knecht, R. Kobayashi, H. Koch, J. Kongsted, A. Krapp, K. Kristensen, A. Ligabue, O. Lutnæs, J. Melo, K. Mikkelsen, R. Myhre, C. Neiss, C. Nielsen, P. Norman, J. Olsen, J. Olsen, A. Osted, M. Packer, F. Pawlowski, T. Pedersen, P. Provasi, S. Reine, Z. Rinkevicius, T. A. Ruden, K. Ruud, V. V. Rybkin, P. Salek, C. C. M. Samson, A. S. de Merás, T. Saue, S. Sauer, B. Schimmelpfennig, K. Sneskov, A. H. Steindal, K. O. Sylvester-Hvid, P. R. Taylor, A. M. Teale, E. I. Tellgren, D. P. Tew, A. J. Thorvaldsen, L. Thøgersen, O. Vahtras, M. A. Watson, D. J. D. Wilson, M. Ziolkowski, and H. Ågren, WIREs Comput. Mol. Sci. **4**, 269 (2014).
[29]DALTON, a molecular electronic structure program, Release DALTON2013.X, 2013. See http://daltonprogram.org.
[30]K. Kaufmann, W. Baumeister, and M. Jungen, J. Phys. B: At. Mol. Opt. Phys. **22**, 2223 (1989).
[31]J. Owrutsky, N. H. Rosenbaum, L. M. Tack, and R. J. Saykally, J. Chem. Phys. **83**, 5338 (1985).
[32]J. D. Hunter, Comput. Sci. Eng. **9**, 90 (2007).
[33]A. Rohatgi, Version 3.3 of WebPlotDigitizer. ZENODO. 10.5281/zenodo.10532, 2014.
[34]R. K. Nesbet, Phys. Rev. A. **14**, 1065 (1976).
[35]M. Stener, P. Decleva, and A. Lisini, J. Electron. Spectrosc. Relat. Phenom. **74**, 29 (1995).
[36]See supplementary material at http://dx.doi.org/10.1063/1.4900545 for the full set of cross section profiles using different basis sets.
[37]A. W. Wishart, Mon. Not. R. Astron. Soc. **187**, 59P (1979).
[38]C. M. Oana and A. I. Krylov, J. Chem. Phys. **131**, 124114 (2009).
[39]M. Venuti and P. Decleva,; J. Phys. B: At. Mol. Opt. Phys. **30**(21), 4839 (1997).
[40]S. Smith and D. Burch, Phys. Rev. **116**, 1125 (1959).
[41]S. Miyake, P. C. Stancil, H. R. Sadeghpour, A. Dalgarno, B. M. McLaughlin, and R. C. Forrey, Astrophys. J. **709**, L168 (2010).
[42]J.-Z. Tang, Y. Wakabayashi, M. Matsuzawa, S. Watanabe, and I. Shimamura, Phys. Rev. A. **49**, 1021 (1994).
[43]H. Sadeghpour, C. Greene, and M. Cavagnero, Phys. Rev. A. **45**, 1587 (1992).
[44]H. J. Kaiser, E. Heinicke, R. Rackwitz, and D. Feldmann, Z. Phys. **270**, 259 (1974).
[45]J. Dellwo, Y. Liu, C. Tang, D. Pegg, and G. Alton, Phys. Rev. A **46**, 3924 (1992).
[46]S. Canuto, J. Geertsen, F. Müller-Plathe, and G. E. Scuseria, J. Phys. B: At. Mol. Opt. Phys. **21**, 3891 (1988).
[47]J. Jose, G. B. Pradhan, V. Radojević, S. T. Manson, and P. C. Deshmukh, J. Phys.: Conf. Ser. **194**, 022096 (2009).
[48]A. Weiss, Phys. Rev. **166**, 70 (1968).
[49]R. Moccia and P. Spizzo, J. Phys. B: At. Mol. Opt. Phys. **23**, 3557 (1990).
[50]D. Feldmann, Z. Phys. A **277**, 19 (1976).
[51]B. Ya'akobi, Phys. Rev. **184**, 246 (1969).
[52]C. A. Ramsbottom, K. L. Bell, and K. A. Berrington, J. Phys. B: At. Mol. Opt. Phys. **27**, 2905 (1994).
[53]D. Moores and D. Norcross, Phys. Rev. A **10**, 1646 (1974).
[54]C. Liu and A. Starace, Phys. Rev. A **59**, 3643 (1999).
[55]A. Mandl, Phys. Rev. A **3**, 251 (1971).
[56]E. Robinson and S. Geltman, Phys. Rev. **153**, 4 (1967).
[57]S. Vacquié, A. Gleizes, and M. Sabsabi, Phys. Rev. A **35**, 1615 (1987).
[58]V. Radojević, H. Kelly, and W. Johnson, Phys. Rev. A **35**, 2117 (1987).
[59]M. Kutzner, J. Robertson, and P. Pelley, Phys. Rev. A **62**, 062717 (2000).
[60]A. Mandl, Phys. Rev. A **14**, 345 (1976).
[61]L. Branscomb, Phys. Rev. **148**, 11 (1966).
[62]L. C. Lee and G. P. Smith, J. Chem. Phys. **70**, 1727 (1979).
[63]P. Hlavenka, R. Otto, S. Trippel, J. Mikosch, M. Weidemüller, and R. Wester, J. Chem. Phys. **130**, 061105 (2009).